A&A 434, 819–825 (2005)
DOI: 10.1051/0004-6361:20042034

Astronomy & Astrophysics

Molecular gas in a $z \sim 2.5$ triply-imaged, sub-mJy submillimetre galaxy typical of the cosmic far-infrared background⋆

J.-P. Kneib[1,2,3], R. Neri[4], I. Smail[5], A. Blain[2], K. Sheth[2], P. van der Werf[6], and K. K. Knudsen[6]

[1] Observatoire Midi-Pyrénées, CNRS-UMR5572, 14 avenue E. Belin, 31400 Toulouse, France
e-mail: jean-paul.kneib@oamp.fr
[2] Caltech-Astronomy, MC105-24, Pasadena, CA 91125, USA
[3] OAMP, Laboratoire d'Astrophysique de Marseille, traverse du Siphon, 13012 Marseille, France
[4] IRAM, 300 rue de la Piscine, 38640 Saint Martin d'Hères, France
[5] Institute for Computational Cosmology, University of Durham, South Road, Durham DH1 3LE, UK
[6] Leiden Observatory, PO Box 9513, NL – 2300 RA Leiden, The Netherlands

Received 21 September 2004 / Accepted 10 January 2005

Abstract. We present the results of observations from the Plateau de Bure IRAM interferometric array of the submillimetre (submm) galaxy SMM J16359+6612 lying at $z = 2.516$ behind the core of the massive cluster A 2218. The foreground gravitational lens produces three images with a total magnification of 45 of this faint submm galaxy, which has an intrinsic submm flux of just $f_{850\,\mu\mathrm{m}} = 0.8$ mJy – placing it below the confusion limit of blank-field surveys. The substantial magnification provides a rare opportunity to probe the nature of a distant sub-mJy submm-selected galaxy, part of the population which produces the bulk of the cosmic far-infrared background at submm wavelengths. Our observations detect the CO(3–2) line in all three images, as well as the CO(7–6) line and the dust continuum at 1.3 mm for the brightest image but only at a 3σ level. The velocity profile of the CO(3–2) line displays a double-peak profile which is well fit by two Gaussians with *FWHM* of 220 km s^{-1} and separated by 280 km s^{-1}. We estimate the dynamical mass of the system to be $\sim 1.5 \times 10^{10}\ M_\odot$ and an H_2 gas mass of $4.5 \times 10^9\ M_\odot$. We identify a spatial offset of $\sim 1''$ between the two CO(3–2) velocity components, again benefiting from the magnification due to the foreground lens, modeling of which indicates that the offset corresponds to just ∼3 kpc in projection at $z = 2.516$. The spatial and velocity properties of these two components are closely related to features detected in previously published Hα spectroscopy. We propose that this source is a compact merger of two typical Lyman-break galaxies with a maximal separation between the two nuclei of about 3 kpc, although a dusty disk explanation is not excluded. This system is much less luminous and massive than other high-redshift submillimetre galaxies studied to date, but it bears a close similarity to similarly luminous, dusty starburst resulting from lower-mass mergers in the local Universe.

Key words. gravitational lensing – cosmology: observations – galaxies: clusters: individual: A2219 – galaxies: high-redshift – infrared: galaxies – galaxies: individual: SMM J16359+6612

1. Introduction

The intensity of the far-infrared background indicates that far-infrared luminous, dusty sources make a significant contribution to the overall energy output from galaxies over the lifetime of the Universe (Puget et al. 1996; Fixsen et al. 1998). This emission may either represent AGN activity, in which case these dusty sources must coincide with an important phase in the growth of super-massive black holes, or dust-obscured star formation, in which case they are responsible for much of the massive star formation and metal enrichment occurring in galaxies at high redshifts. To understand the nature and properties of this activity we need to resolve the background into individual sources, suitable for more detailed study. For sources contributing to the peak of the far-infrared background, 100–200 μm, this work relies on space-based observatories, with modest apertures and correspondingly bright confusion limits, resulting in the resolution and identification of only a small (and hence perhaps unrepresentative) fraction of the galaxies contributing to the background, $\lesssim$10% (Dole et al. 2001).

Atmospheric windows at longer wavelengths allow larger-aperture ground-based telescopes to resolve a greater fraction of the cosmic background at millimetre (mm) and submillimetre (submm) wavelengths. Continuum surveys in the submm/mm wavebands using both SCUBA on the JCMT and MAMBO on the IRAM 30-m have identified several hundred of submm/mm galaxies (hereafter SMGs) to date. However, again the relatively coarse resolution of these telescopes, $\gtrsim 10''$,

⋆ Based on observations carried out with the IRAM Plateau de Bure Interferometer. IRAM is supported by INSU/CNRS (France), MPG (Germany) and IGN (Spain).

results in source confusion limiting these observations to identifying individual sources brighter than $\gtrsim$2 mJy at 850 μm (e.g. Blain et al. 2002). Thus most of the best-studied samples of SMGs have 850-μm fluxes in the range 4–10 mJy (e.g. Ivison et al. 2002; Webb et al. 2003; Bertoldi et al. 2000), which have also been the focus of recent work to determine the redshift distribution of the bright submm population, yielding a median redshift of $z = 2.3$ (Chapman et al. 2003, 2004). Unfortunately, once again, this population may not be completely representative as they only contribute around 30% of the far-infrared background at submm wavelengths (Smail et al. 2002).

To access the submm sources which are responsible for the bulk of the cosmic submillimetre background (and hence contain most of the star-formation or AGN activity) we need to probe down to flux densities below 1 mJy at 850 μm (Smail et al. 2002; Cowie et al. 2002). These sources are fainter than the confusion limit of blank-field submm surveys making them impossible to identify or study individually in detail from such samples. Nevertheless, they are amenable to study by exploiting the natural gravitational magnification of massive clusters of galaxies (Kneib et al. 1996; Blain 1997). The magnification provided by the cluster lens both boosts the brightness of the source and provides a finer effective beam size – reducing the effects of confusion – and bringing the sub-mJy submm population within reach of current telescopes. This technique was used for the first extragalactic submm surveys (Smail et al. 1997; Blain et al. 1999; Chapman et al. 2000; Cowie et al. 2002) and has provided a powerful route to understand the nature of this population of distant, faint galaxies (Blain et al. 2002) as well as other high-redshift galaxy populations (e.g. Baker et al. 2004). These studies show that SMGs with 850-μm fluxes within a factor of two of 1 mJy have a surface density of $\sim$3–4 arcmin^{-2} and produce roughly half of the submm background (Smail et al. 2002). Combining these SMGs with the population of brighter sources accessible in blank-field surveys, we can trace the properties of SMGs that contribute the majority of the background radiation at submm wavelengths.

The first redshifts of SMGs were obtained for sources lensed by massive galaxy clusters (Ivison et al. 1998, 2000) and cluster lenses continue to aid in the spectroscopic identification of this population (e.g. Frayer et al. 2003; Kneib et al. 2004a; Borys et al. 2004). These redshifts enable us to search for the corresponding line emission from cold gas within these galaxies – providing valuable information on the dynamics of these systems, the role played in these by the baryonic component and the extent of the gas reservoir available to power future activity. The first such observations targeted the rotational transitions of ^{12}CO gas with the OVRO (Frayer et al. 1998, 1999; Ivison et al. 2001) and IRAM arrays (Downes & Solomon 2003; Neri et al. 2003; Genzel et al. 2003). Similar work on brighter blank-field SMGs has built upon the recent SMG redshift survey of Chapman et al. (2003, 2004), in a major programme to detect CO line emission from a large sample of bright submm galaxies with the IRAM PdBI (Neri et al. 2003; Greve et al. 2005). However, all of the submm galaxies studied in CO so far (both cluster lens and blank-field targets) are intrinsically luminous systems, none are from the mJy-submm population which dominates the far-infrared background.

Recently, Kneib et al. (2004a) and Borys et al. (2004) have discovered two strongly magnified and multiply-imaged SMGs at $z = 2.516$ and $z = 2.911$ lensed respectively by the massive clusters A 2218 and MS 0451−05. These sources have intrinsic submm fluxes below 1 mJy, but with magnifications greater than 10 for at least two of the three detected images in each system. Their CO emission should be within reach of interferometric observations with current instruments.

In this paper, we present recent observations with the IRAM array of redshifted molecular CO emission in the 3-mm and 1.3 mm bands of the triply-imaged sub-mJy SMG SMM J16359+6612 at $z = 2.516$. Interferometric CO observations of this system have recently been published by Sheth et al. (2004) using the OVRO array, although the significance of their detections is lower than that described here. We present our observations in Sect. 2, describe our analysis and results in Sect. 3 and give our conclusions in Sect. 4. Throughout the paper we will assume an $\Omega = 0.27$, $\Lambda = 0.73$ cosmology with $H_0 = 71$ km s^{-1} Mpc^{-1}. At a redshift of $z = 2.516$ the angular scale is thus 8.18 kpc/arcsec. All quoted coordinates are in J2000.

2. Observations

We used the six antennas of the IRAM PdBI to image the CO(3–2) and CO(7–6) lines of SMM J16359+6612 (named hereafter SMM1 in the text) at a redshift of 2.516 (Kneib et al. 2004a). As the primary beam of the antenna is about 50″ and 21″ at the frequency of redshifted CO(3–2) and CO(7–6) (98.405 GHz and 229.544 GHz respectively), three different positions around SMM J16359+6612 were targeted to completely map the three different images. We have approximately 16 h on-source at 3 mm and 5 h at 1.3 mm (after flagging low-quality visibilities) for the central pointing at α = 16:35:54.5, δ = 66:12:31, $\sim$9 h at 3 mm on the southern pointing (α = 16:35:51.7, δ = 66:12:10) and $\sim$2 h on the northern one (α = 16:35:55, δ = 66:12:50). No useful integration time was obtained at 1.3 mm at the latter two positions. All these observations were carried out in the D configuration between November 2003 and June 2004. To improve the 1.3 mm continuum detection, we also used data from an earlier $\sim$5 h track which we observed on December 10, 2001 at 237.191 GHz with the phase tracking center at α = 16:35:54.1, δ = 66:12:23. We used 1637+574 as phase and amplitude calibrator, and 0420−014, 0923+392, 3C 84 and MWC349 as bandpass calibrators and to define the flux density scale. We estimate that the flux densities at 3 mm are accurate to better than 10%, and to better than 20% at 1.3 mm.

Our 3-mm spectra provide velocity coverage extending from −850 to +850 km s^{-1} around a zero-LSR redshift of $z = 2.514$ for each of the three sources. 3-mm line visibilities were averaged in frequency and combined to produce natural-weighted dirty maps. These were cleaned using the Clark algorithm, restored with a Gaussian beam of 5.9″ × 5.4″ with a position angle of 98°, and corrected for primary beam attenuation. Natural-weighted dirty maps were also made of the continuum emission at 3 mm and 1.3 mm by uv-averaging over

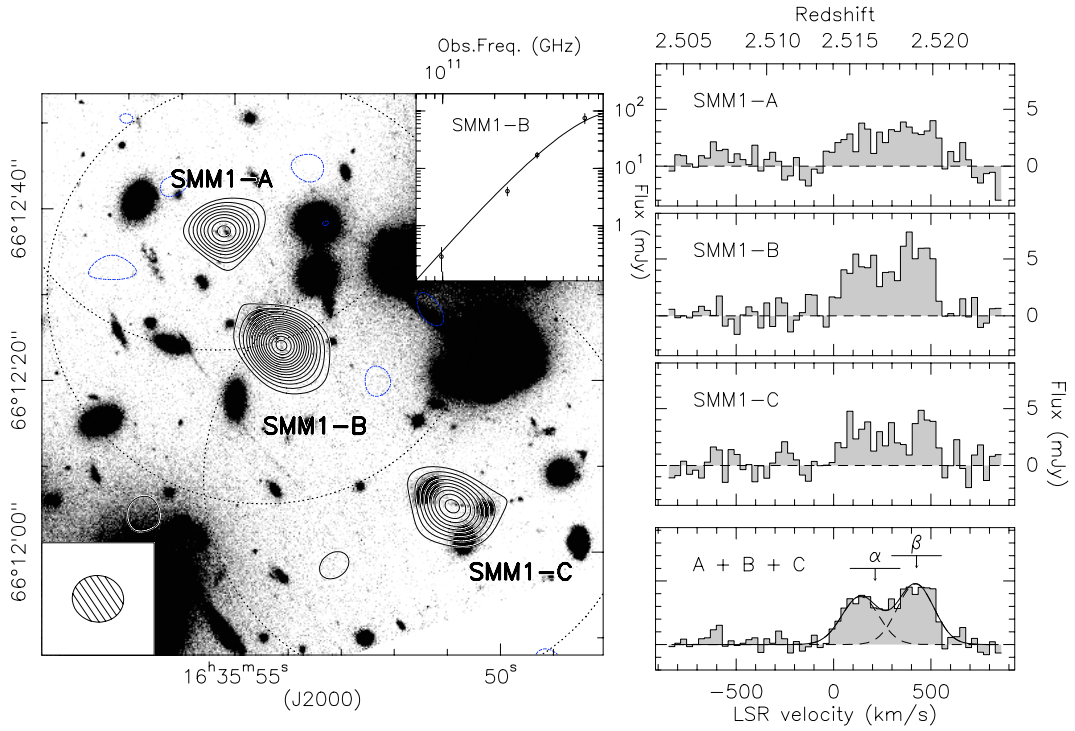

Fig. 1. (*Left*) The IRAM/PdBI ^{12}CO(3–2) map of SMM J16359+6612 (=SMM1) superposed on the *HST* F814W image of A 2218. We clearly identify the images SMM1-A, B and C, all three well centered on their optical counterparts. The contours start at $\pm 2\sigma$ and are plotted in steps of σ = 0.24 mJy. The large dashed circle give the half-power size of the primary beam of the PdBI at 98 GHz at the three pointing positions. The synthesized beam is displayed in the lower-left corner and has a *FWHM* of 5.9″ × 5.4″ and a position angle of 98°. We stress that the effective beam size in the source plane is roughly 20 times smaller along the shear direction (PA of ∼40°) in the vicinity of SMM1-B. The inset at top right shows the spectral energy distribution of SMM1-B from the 3 mm, 1.3 mm, 850 μm and 450 μm measurements (the 450- and 850-μm fluxes density is measured from the SCUBA discovery maps in Kneib et al. 2004a). (*Right*) This panel displays (*from top to bottom*) the velocity profile of the three different submm images SMM1-A, B and C, and of the sum of these three spectra. A double-peak profile is clearly observed for SMM1-B and -C, as well as in the sum of all three components (*bottom panel*). Fitting two Gaussians to the sum of the three velocity profiles indicates that the two components are separated by ∼280 km s^{-1}. There is weak evidence that the higher-velocity component has a higher flux density, but a narrower width. For comparison, we mark on the redshifts of the two features identified by Kneib et al. (2004a) from their analysis of the *HST* imaging and Hα spectroscopy of this system: α and β (see Fig. 2).

the line-free channels. We estimate the absolute precision of the astrometry of our maps as 0.2–0.3″, sufficient to precisely locate the CO emission relative to sources in the *HST* imaging. The astrometry of the *HST* imaging is tied through wide-field ground-based images to the USNO reference frame, yielding absolute astrometry at the 0.2″ level (Kneib et al. 2004a).

3. Analysis and results

3.1. The CO(3–2) line

We detect the CO(3–2) line at high significance in all three images and show the velocity-integrated line map and spectra in Fig. 1, with tabulated information in Table 1. The flux-weighted mean redshifts of the lines (integrated across the *FWZI* from −10 to 540 km s^{-1}) in the three images are identical – $z_{\rm CO}$ = 2.5174 ± 0.0002. The ratio of CO(3–2) line intensities for the three images roughly corresponds to that seen for their 850-μm and K-band fluxes from Kneib et al. (2004a): $I_{\rm A/B}$ = 0.67 ± 0.18 and $I_{\rm C/B}$ = 0.63 ± 0.19, compared to 0.64, 0.53 and 0.53, 0.40 from the 850-μm and K-band respectively. These flux ratios are all consistent with the predicted magnification ratios from the lens model of the cluster: $M_{\rm A/B}$ = 0.64 ± 0.14 and $M_{\rm C/B}$ = 0.41 ± 0.12. The CO(3–2) line widths measured from the spectrum of each image are also all large, corresponding to *FWZI* of 500 km s^{-1}. These observations allow us for the first time to categorically state that all three sources, SMM1-A, B and C, represent images of a single background object.

Compared to the OVRO observations of SMM J16359+6612 in Sheth et al. (2004), we measure a slightly lower total integrated CO flux: 5.75 ± 0.25 Jy km s^{-1} (versus 6.3 ± 0.2 Jy km s^{-1}), and a slightly higher redshift: z = 2.5174 ± 0.0002 (compared to z = 2.5168 ± 0.0003). In both cases the differences are relatively minor and the higher signal to noise of our detections would suggest our results are the more reliable.

We can also exploit the better signal-to-noise of our observations to look in more detail at the structure in the CO(3–2) lines. We find that the CO(3–2) line profiles display a characteristic double-peaked profile in SMM1-B and SMM1-C, while the structure of the spectrum of SMM1-A is less obviously bimodal. We combine the three spectra to increase the signal-to-noise yet further (assuming that differential magnification effects across the source are small, which

Table 1. Observed properties of the three images of SMM J16359+6612, uncorrected for lens magnification. We list the centroids of the CO(3–2) emission and the flux-weighted redshifts derived for each image. $I_{CO(3-2)}$ is the velocity-integrated line intensity from the Gaussian fit (see text). I_B/I_R is the corresponding ratio of the blue-shifted to red-shifted CO(3–2) line emission. $I_{CO(7-6)}/I_{CO(3-2)}$ is the intensity ratio of CO(7–6) versus CO(3–2) line emission in the 0–370 km s^{-1} window (with respect to $z = 2.514$, Fig. 1). $S_{1.3\ mm}$ is the flux density of the 1.3 mm continuum detected towards SMM1-B, the brightest component. The last column gives the magnification factor at the position of the three images derived from the detailed mass model of the foreground cluster by Kneib et al. (2004a,b).

ID	α,δ (J2000)	z	$I_{CO(3-2)}$ (Jy km s^{-1})	I_B/I_R	$I_{CO(7-6)}/I_{CO(3-2)}$	$S_{1.3\ mm}$ (mJy)	Mag
A	16:35:55.18 66:12:37.2 (±0.2″)	2.51740	1.67 (±0.13)	0.74 (±0.02)	2.8 (±1.2)	...	14 (±2)
B	16:35:54.10 66:12:23.8 (±0.2″)	2.51741	2.50 (±0.12)	0.74 (±0.02)	1.4 (±0.4)	3.0 (±0.7)	22 (±2)
C	16:35:50.96 66:12:05.5 (±0.3″)	2.51744	1.58 (±0.17)	0.88 (±0.02)	...	...	9 (±2)

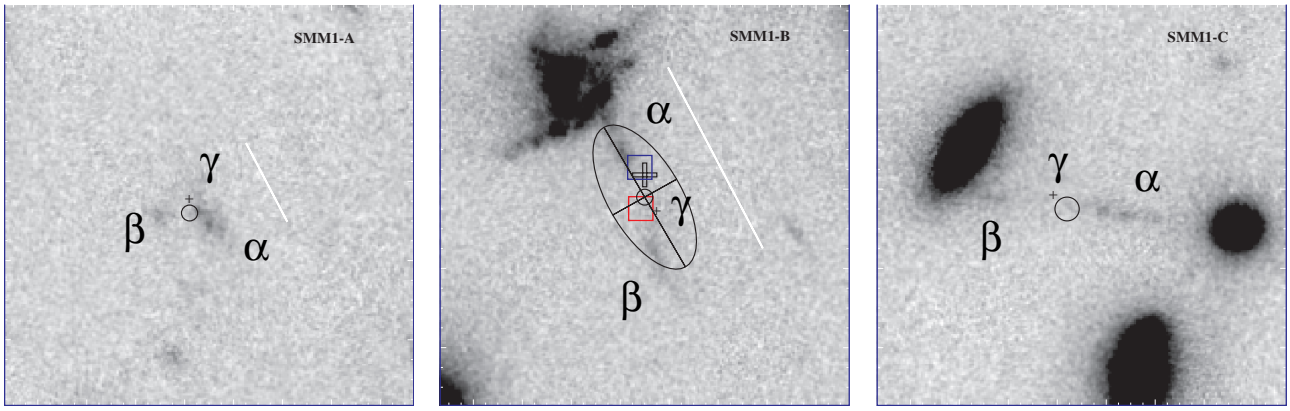

Fig. 2. 10″ × 10″ regions from the *F*814*W*-band *HST* WFPC2 image of the triply-imaged submm source SMM J16359+6612, showing images A, B and C (*from left to right*). We overlay on each the position of the CO(3–2) line emission centroid as measured from our data (small circle), the relative uncertainty on these positions is ≲0.3″. For component SMM1-B (*middle panel*) we plot the size of the beam-corrected CO(3–2) profile as an ellipse and we also indicate the centroid of the blue-shifted (≤220 km s^{-1}) and red-shifted (≥280 km s^{-1}) velocity components of the line (respectively top and bottom squares) and the location of the 1.3 mm continuum emission (large open cross). Note that every image of SMM1 comprises a NIR source (γ, marked as a cross) which is bracketed by two bluer features visible in these *F*814*W* images (α and β). For SMM1-A and SMM1-B we have indicated by white lines the extent of the Hα line observed in the NIRSPEC data of Kneib et al. (2004a). The resolution of the *HST* images are ∼0.15″; North is up and East is to the left.

should be correct for a compact object) as shown in Fig. 1. We fit the combined velocity profile using a two Gaussian fit to determine the redshift, width and relative intensity of the two velocity components. We find that the velocity profile requires both Gaussians for an adequate fit, each with widths of 220 ± 20 km s^{-1} and separated by 280 ± 20 km s^{-1}. The flux ratio between the blue-shifted and red-shifted components is $I_B/I_R = 0.74 \pm 0.02$ (Table 1). The redshifts of the two velocity components are $z_{blue} = 2.5156 \pm 0.0002$ and $z_{red} = 2.5189 \pm 0.0002$. We note that Kneib et al. (2004a) reported $z = 2.5165 \pm 0.0015$ for the Hα redshift of the optical structure α, and $z = 2.5190 \pm 0.0015$ for feature β in SMM1-B (Fig. 2) and return to this point below.

To investigate these two velocity components in more detail and search for changes in size or position with velocity, the visibilities were fitted first with elliptical Gaussians. Although we could not resolve SMM1-A or -C, SMM1-B (the most magnified image) is best fit by an elliptical Gaussian with a beam-corrected size of 4.1 ± 0.6″ × 1.8 ± 1.0″ and a position angle of 30 ± 13° – this is plotted as an ellipse in the central panel of Fig. 2. We note that this agrees well with the size and orientation of the optical counterpart of this system in Fig. 2. Correcting for the lensing magnification, using the well-constrained mass model of A 2218 (Kneib et al. 1996, 2004b; Ellis et al. 2001), this ellipse maps to a linear size of ∼3 × 1.5 kpc in the source plane (there is some complex, but weak, dependence according to the adopted position angle). Note that the tentative resolution of SMM1-B claimed by Sheth et al. (2004) has a nearly orthogonal orientation to that derived here (PA of −68°), transverse to the local shear direction and hence the lensing-corrected size they estimate is significantly larger than our measurement: 12 kpc versus 3 kpc.

To investigate whether the red-shifted and blue-shifted velocity components originate from two different spatial positions, for the blue-shifted emission we integrated the velocity map for all three images from ∼20–230 km s^{-1} (note the reference redshift is $z = 2.5140$) and for the red-shifted emission from ∼300–510 km s^{-1}. Again for SMM1-A and SMM1-C, no strong distinction could be made in the position of the blue-shifted and red-shifted velocity channels. However, for the SMM1-B component the two velocity components show a well-detected spatial separation (see Table 2 and Fig. 2) between the blue-shifted and red-shifted gas. The two components are separated along the major axes of the CO(3–2) emission and the optical counterpart (Fig. 2). Based on just the spatial information, and allowing for the ∼0.4″ uncertainty in

Table 2. The properties of the velocity components of the CO(3–2) and Hα lines of SMM1-B. The coordinate offsets are computed with respect to the position of the optical feature α within SMM1-B (α = 16:35:54.19, δ = 66:12:24.92, Kneib et al. 2004a) – note there the relative astrometry of the optical and CO maps is uncertain at the ∼0.4″ level. CO(3–2) and Hα velocities are relative to the Hα redshift of α of z = 2.5165 (corresponding to +210 km s^{-1} relative to z = 2.5140).

SMM1-B component	$\Delta\alpha$ (″)	$\Delta\delta$ (″)	z	v km s^{-1}	Δv km s^{-1}
CO(3–2) blue+red	−0.56 (±0.16)	−1.14 (±0.16)	2.5172 (±0.0002)	70 (±20)	440 (±80)
CO(3–2) blue	0.42 (±0.20)	−0.37 (±0.20)	2.5156 (±0.0002)	−70 (±20)	220 (±50)
α (Hα)	0.0	0.0	2.5165 (±0.0015)	0	280 (±60)
CO(3–2) red	0.45 (±0.17)	−1.41 (±0.17)	2.5189 (±0.0002)	210 (±20)	220 (±50)
β (Hα)	0.78 (±0.10)	−2.51 (±0.10)	2.5190 (±0.0015)	220 (±60)	280 (±60)

the relative astrometry of the CO and optical maps, we suggest that the blue-shifted component of the SMM1-B CO(3–2) line is likely associated with the optical feature α and the red-shifted component with the optical feature β. If this is indeed the case, then the blue- and red-shifted components of the CO(3–2) emission in SMM1-B are both spatially and kinematically coincident with the optical structures α and β cataloged by Kneib et al. (2004a). Alternatively, the CO(3–2) line could be associated to a smaller rotating structure closer and around component γ, however with no strong optical or Hα counterpart, which makes this possibility less likely but not impossible. Higher resolution millimeter observation of this system should confirm the true nature of this system.

3.2. The CO(7–6) line

The velocity coverage of our parallel observations of the CO(7–6) SMM J16359+6612 in the 1.3 mm band extends from −380 km s^{-1} to +380 km s^{-1} (corresponding to the redshift interval z = 2.510–2.518). Thus, only part (about 70%) of the expected broad CO(7–6) line is covered by the frequency setup. The noise level in the 1.3 mm band is also relatively high and does not allow a high confidence level measurement. Within this limited 1.3 mm window we measure a CO(7–6) flux of $I_{\rm CO(7-6)}$ = 3.3 ± 1.4 Jy km s^{-1} for SMM1-A and $I_{\rm CO(7-6)}$ = 2.5 ± 0.7 Jy km s^{-1} for SMM1-B. In order to quote representative measurements of the CO(7–6)/CO(3–2) line ratio, we have computed the integrated flux in the redshift window from z = 2.5140 to z = 2.5185 for the two lines CO(3–2) and CO(7–6) at the position of SMM1-A and SMM1-B. The derived flux ratios are: $I_{\rm CO(7-6)}/I_{\rm CO(3-2)}$ = 2.8 ± 1.2 for SMM1-A, and $I_{\rm CO(7-6)}/I_{\rm CO(3-2)}$ = 1.4 ± 0.6 for SMM1-B (the larger error for SMM1-A is mainly due to the larger primary beam correction at 1.3 mm for this source). These measurements should be reduced by ∼50% to account for the contribution from continuum emission (∼3 mJy) within the velocity window used to integrate the CO(7–6) line.

The mean CO(7–6) to CO(3–2) flux ratio for SMM1-A/B is comparable to the value $I_{\rm CO(7-6)}/I_{\rm CO(3-2)}$ = 1.14 ± 0.20 found for the lensed SMG, SMM J14011+0252 at z = 2.565 (Downes & Solomon 2003). As in SMM J14011+0252, the strength of CO(7–6) relative to CO(3–2) indicates both a relatively high temperature, T ∼ 50 K, and high H_2 density, ∼10^3 cm^{-3}, for the gas reservoir in this galaxy.

3.3. Continuum emission

We detected weak continuum emission towards SMM1-B at α = 16:35:54.1, δ = 66:12:24.36. The flux density is 3.0 ± 0.7 mJy at 1.3 mm (237 GHz), and within our astrometric accuracy (0.2″–0.3″) this position (Fig. 2) is coincident with the integrated CO(3–2) emission from SMM1-B (the synthetised beam has a size of 1.9″ × 1.5″ at a PA of −37°). We also detect a much weaker continuum source at this precise position in our 3 mm (98 GHz) data, with a flux density of 0.29 ± 0.13 mJy. We fit the spectral energy distribution (SED) of the dust emission using these two flux points, in combination with the 450- and 850-μm values from Kneib et al. (2004a), see inset panel in Fig. 1. We determine a spectral index of $\sim\nu^{3.2}$ from the slope of the SED between 850 μm and 3 mm – characteristic of optically thin dust emission. The dust emissivity index is thus $\beta \sim 1.2$, very similar to that derived for bright *IRAS* galaxies locally ($\beta \sim 1.3 \pm 0.2$, Dunne et al. 2000).

We can also estimate the temperature from the fit to the four long-wavelength photometric observations of the SMM1-B, this is determined rather accurately, as $T_{\rm d}$ = 51 ± 3 K. Including the Metcalfe et al. (2003) ISO limit we have $T_{\rm d}$ = 48 ± 3 K for SMM1-B data assuming β = 1.5. We can use this value, along with the dust emissivity index and the magnification-corrected 850 μm flux (which is our most precise flux measurement) to estimate the dust mass, assuming a dust mass opacity coefficient, $\kappa_{\rm d}$ = 0.077 m^2 Kg^{-1} at 850 μm (Dunne et al. 2000). This calculation yields a mass of $(1.9 \pm 0.3) \times 10^7\ M_\odot$, subject to the considerable uncertainty in the opacity coefficient.

The corresponding total bolometric luminosity is 1.6 ± $0.4 \times 10^{12}\ L_\odot$. Hence, although intrinsically faint at millimetre and submillimetre wavelengths, owing to its high dust temperature, SMM J16359+6612 is still a relatively luminous galaxy. It will be interesting to include *Spitzer Space Telescope* data to confirm and better constrain the dust temperature.

4. Conclusions

We have compared the results of our PdBI observations of SMM J16359+6612 with those derived from shallower data taken with the OVRO array by Sheth et al. (2004). We find broad agreement between these datasets, some discrepancies do exist but can be attributed to the lower signal to noise of

the OVRO data. The high-fidelity CO maps provided by the IRAM PdBI (in particular due to its better coverage of all 3 sources) add significantly more detail to address the nature and properties of this unique source.

A detailed analysis of the CO(3–2) velocity profile shows a double-peak structure with a significant spatial offset between the blue- and red-shifted gas components. Comparing the positions and redshifts of these two gas components with the complex optical/near-infrared morphology discussed by Kneib et al. (2004a), we tentatively identify the kinematic components seen in CO(3–2) with two features visible in the *HST* imaging of this system: α and β (Kneib et al. 2004a). We note that the CO(3–2)/Hα luminosity ratio is much larger for component β, either due to stronger dust obscuration in β or because of slit-losses in the Hα observations resulting from a misalignment of the slit across the source. Near-infrared integral field spectroscopy of this SMG to measure the spatial structure of the Hα line will be essential to better determine the relative distribution of cold and ionised gas across this system.

The spatial separation of the two CO(3–2) components is ∼1.5 kpc (with a maximal extent of ∼3 kpc) on the sky (once corrected for the lensing magnification). This scale suggests we are either seeing a molecular gas disk or ring within a single galaxy, or two strongly interacting gas-rich components of a merger. The latter possibility is favored, as the three optical/NIR component α, β and γ are not co-linear, and thus are not representative of a stable disk. We can use the spatial and velocity information (a rotation velocity of 150 km s^{-1} at a scale of 3 kpc) to estimate the dynamical masses in these two scenarios. We derive a mass of $M_{\rm dyn} = (0.8 \pm 0.2) \times 10^{10}$ $M_\odot$ at a radius of 1.5 kpc if the gas is distributed in a ring/disk, and $M_{\rm dyn} = (1.5 \pm 0.3) \times 10^{10}$ $M_\odot$ within the same aperture if the system is a merger (we assume a 90° inclination here, otherwise both of these estimates need to be scale with $(\sin i)^{-2}$).

SMM J16359+6612 is the third SMG in which spatially-resolved CO emission has been detected, the other two being SMM J02399−0135 at $z = 2.81$ (Genzel et al. 2003) and SMM J14011+0252 at $z = 2.56$ (Downes & Solomon 2003; Ivison et al. 2001). SMM J02399−0135 shows a double-peaked CO(3–2) line with a spatial offset of 10 kpc and 400 km s^{-1} between the components, while SMM J14011+0252 has only a single velocity component (*FWHM* of 200 km s^{-1}) with a size of ∼3 kpc (adopting the magnification factor for the lensing configuration for this source from Swinbank et al. 2004). The gas distribution in SMM J14011+0252 is thus very similar in scale (as well as having similar dynamical and far-infrared luminosities) to SMM J16359+6612, while SMM J02399−0135 is both significantly more luminous, larger and more massive. However, the dense gas detected in all three systems has a much wider distribution than the comparable component in local Ultraluminous Infrared Galaxies (ULIRGs), ∼0.3 kpc (Downes & Solomon 1998).

With our assumed cosmology, the total CO(3–2) line flux converts to an observed CO(3–2) luminosity of SMM1-B of $(8.2 \pm 0.4) \times 10^{10}$ K km s^{-1} pc^2, correcting from the lensing magnification the intrinsic CO(3–2) luminosity is then $(3.7 \pm 0.2) \times 10^9$ K km s^{-1} pc^2. The CO(3–2) luminosity we measure is roughly half of the value found for Arp 220 (Solomon et al. 1997), although Arp 220 is comparably luminous in the far-infrared to SMM J16359+6612.

Using the relation from Solomon et al. (1997) and Downes & Solomon (1998) which indicate a CO luminosity to gas mass conversion factor of ∼0.8–1.6 $M_\odot$ (K km s^{-1} pc^2)$^{-1}$ we derive a molecular gas mass of $(4.5 \pm 1.0) \times 10^9$ $M_\odot$, giving a gas mass surface density of $\gtrsim 10^3$ $M_\odot$ pc^{-2}. Comparing this to our dynamical estimates suggests a gas mass fraction of ∼60% for a disk/ring-like structure or ∼30% for a merger. Combined with our earlier estimate of the dust mass, this indicates a dust-to-gas ratio of 0.004 ± 0.001, similar to that seen in local galaxies (Dunne et al. 2000).

The star-formation rate estimated from the far-infrared luminosity by Kneib et al. (2004a) is ∼500 $M_\odot$ yr^{-1} for stars >0.1 $M_\odot$ (note that in contrast the Hα-derived SFR is only ∼10 $M_\odot$ yr^{-1}, before correcting for extinction and slit losses). Taking the far-infrared estimate of the SFR this indicates that the current activity cannot continue at its present level for more than another 10 Myr. Even allowing for the fact that the far-infrared luminosity is dominated by the emission from the most massive stars – thus allowing us to use an IMF dominated by massive stars or even to adopt a top-heavy IMF (Baugh et al. 2005) – would only extend this lifetime to ∼50 Myr. These estimates are comparable to the crossing-time of the system, indicating that the starburst is likely to be an instantaneous non-equilibrium event – arguing against a stable disk/ring configuration for the gas within this system – and suggesting instead that we are seeing the results of a tidal-induced starburst in a pair of merging galaxies (α and β). The rest-frame UV/optical morphology of this system suggests that a highly-obscured starburst is being triggered in the overlap region between the two galaxies (component γ in Kneib et al. 2004a) as is commonly seen in low-redshift mergers.

We can also compare the ratio of the far-infrared luminosity produced by SMM J16359+6612 to its H_2 gas mass: $L_{\rm FIR}/M_{\rm H_2} \sim 320$. This is roughly ten time higher than seen in Arp 220 (or comparably luminous galaxies locally, Dunne et al. 2000; Downes et al. 1997). This high ratio indicates that the activity in SMM J16359+6612 is far more efficiently or vigorously using the available gas supply than is typical in starburst systems at $z \sim 0$. This may either result from special physical conditions associated with intense starbursts at high redshifts. For example the activity could derive from wide spread instabilities in large gas disks triggered by dynamical interactions, which are not possible in comparably massive and gas-rich, but bulge-stabilised, systems at low redshift. Alternatively, the high $L_{\rm FIR}/M_{\rm H_2}$ could reflect far-infrared emission from a highly-obscured AGN – although there are no spectral signatures of an AGN. Turning this argument around – the free availability of gas to power such nuclear activity, but the apparent lack of any signatures of an AGN in the spectroscopy of this source from Kneib et al. (2004a), may indicate that the central black hole(s) in this system (and the associated bulge) has not yet grown large enough to produce a luminous AGN. The current interaction, and any subsequent mergers with the other close companions in the compact and dynamically-cold group around SMM J16359+6612 (the Lyman-break galaxies #384

and #273, Kneib et al. 2004a), will provide the opportunity for substantial bulge growth and associated accretion-driven activity from the central black hole of this system.

To judge how the properties of this relatively low-luminosity SMG compare to the other well-studied population of moderately active galaxies at $z \gtrsim 2$, the Lyman-break population (Steidel et al. 2004), we can compare the parameters we measure for SMM J16359+6612 to those measured for a similarly highly magnified Lyman-break galaxy: cB58 at $z = 2.73$ (Baker et al. 2001, 2004). cB58 has a SFR of just 20 $M_\odot$ yr^{-1}, an inferred gas mass of $\sim 7 \times 10^9$ $M_\odot$, a dynamical mass of $\sim 1\text{–}2 \times 10^{10}$ $M_\odot$, a gas fraction of $\sim 0.3\text{–}0.7$ and an average gas surface mass density of $\Sigma \sim 500$ $M_\odot$ pc^{-2} (all within a 2 kpc radius, Baker et al. 2004). These estimates are very similar to those we derive for SMM J16359+6612 with the exception that SMM J16359+6612 has an order of magnitude higher instantaneous star-formation rate and a marginally higher gas surface density. Taken with our previous suggestion that SMM J16359+6612 represent a merger, the comparison to cB58 suggests that it may be a merger between two typical Lyman-break galaxies. The merger has increased the gas density within the system and triggered a burst of activity which will quickly use up the bulk of the gas reservoir in a single event (which would have otherwise fueled a more sedate level of activity for 100's Myr).

In summary, several of the properties of SMM J16359+6612 appear to resemble those of similar luminosity merging/interacting systems at low redshift, e.g. the dust spectral index, dust-to-gas ratio, presence of an obscured starburst in the overlap zone between the merging components, etc. However, the ratio of far-infrared luminosity to gas mass and the physical extent of the apparently high-density gas reservoirs in the progenitors are both an order of magnitude larger than for local systems. As SMM J16359+6612 is an order of magnitude fainter at submm wavelengths than other distant SMGs studied in detail to date, and also less massive, it is not yet clear how many of these similarities and differences to low-redshift ULIRGs will carry over to the bulk of the SMG population. However, we stress that the properties of SMM J16359+6612 may be more representative of the high-redshift population which produces a large fraction of the submm cosmic extragalactic background in the submm waveband, and hence are more relevant for understanding the evolutionary behaviour of the majority of the oldest stellar components in local galaxies: bulges. The fact that the properties of this system are more likely to resemble those expected for a merger of two typical Lyman-break galaxies suggests a link between these two populations (at least for sub-mJy SMGs). We also note that SMM J16359+6612 has yet to be observed at the highest spatial resolution achievable with the IRAM array – these will provide a further factor of ten improvement in the resolution – probing the gas distribution within this rare example of the sub-mJy submm galaxy population at sub-kpc scales, which will fully characterize the nature of this system.

Acknowledgements. We thank the anonymous referee for its comments which help to improve this paper. We acknowledge useful discussion with Rob Ivison and Colin Borys. We also thank Michael Grewing for according us Director Discretionary time which helped us to secure these results. J.P.K. acknowledges support from CNRS and Caltech, and thanks IRAM staff for its hospitality during his stay in Grenoble while working on these data. I.R.S. acknowledges support from the Royal Society. A.W.B. acknowledges support from the NSF under grant AST-0205937, the Research Corporation and the Alfred P. Sloan foundation.

References

Baker, A. J., Lutz, D., Genzel, R., Tacconi, L. J., & Lehnert, M. D. 2001, A&A, 372, L37
Baker, A. J., Tacconi, L. J., Genzel, R., Lehnert, M. D., & Lutz, D. 2004, ApJ, 604, 125
Baugh, C. M., Lacey, C. G., Frenk, C. S., et al. 2005, MNRAS, 356, 1191
Bertoldi, F., Carilli, C. L., Menten, K. M., et al. 2000, A&A, 360, 92
Blain, A. W. 1997, MNRAS, 290, 553
Blain, A. W., Kneib, J.-P., Ivison, R. J., & Smail, I. 1999, ApJ, 512, L87
Blain, A. W., Smail, I., Ivison, R. J., Kneib, J.-P., & Frayer, D. T. 2002, Phys. Rep., 369, 111
Borys, C., Chapman, S., Donahue, M., et al. 2004, MNRAS, 352, 759
Chapman, S. C., Blain, A. W., Ivison, R. J., & Smail, I. 2003, Nature, 422, 695
Chapman, S. C., Blain, A. W., Smail, I., & Ivison, R. J. 2004, ApJ, 614, 671
Cowie, L. L., Barger, A. J., & Kneib, J.-P. 2002, AJ, 123, 2197
Dole, H., Gispert, R., Lagache, G., et al. 2001, A&A, 372, 364
Downes, D., & Solomon, P. M. 1998, ApJ, 507, 615
Downes, D., & Solomon, P. M. 2003, ApJ, 582, 37
Dunne, L., Eales, S., Edmunds, M., et al. 2000, MNRAS, 315, 115
Ellis, R., Santos, M. R., Kneib, J., & Kuijken, K. 2001, ApJ, 560, L119
Fixsen, D. J., Dwek, E., Mather, J. C., Bennett, C. L., & Shafer, R. A. 1998, ApJ, 508, 123
Frayer, D. T., Ivison, R. J., Scoville, N. Z., et al. 1998, ApJ, 506, L7
Frayer, D. T., Ivison, R. J., Scoville, N. Z., et al. 1999, ApJ, 514, L13
Frayer, D. T., Armus, L., Scoville, N. Z., et al. 2003, AJ, 127, 728
Genzel, R., Baker, A. J., Tacconi, L. J., et al. 2003, ApJ, 584, 633
Greve, T. R., Bertoldi, F., Smail, I., et al. 2005, MNRAS, in press
Ivison, R. J., Smail, I., Le Borgne, J.-F., et al. 1998, MNRAS, 298, 583
Ivison, R. J., Greve, T. R., Smail, I., et al. 2002, MNRAS, 337, 1
Kneib, J.-P., Ellis, R. S., Smail, I., Couch, W. J., & Sharples, R. M. 1996, ApJ, 471, 643
Kneib, J., van der Werf, P. P., Kraiberg Knudsen, K., et al. 2004a, MNRAS, 349, 1211
Kneib, J., Ellis, R. S., Santos, M. R., & Richard, J. 2004b, ApJ, 607, 697
Neri, R., Genzel, R., Ivison, R. J., et al. 2003, ApJ, 597, L113
Puget, J.-L., Abergel, A., Bernard, J.-P., et al. 1996, A&A, 308, L5
Sheth, K., Blain, A. W., Kneib, J.-P, et al. 2004, ApJ, 614, L5
Smail, I., Ivison, R. J., & Blain, A. W. 1997, ApJ, 490, 5
Smail, I., Ivison, R. J., Kneib, J.-P., et al. 1999, MNRAS, 308, 1061
Smail, I., Ivison, R. J., Blain, A. W., & Kneib, J.-P. 2002, MNRAS, 331, 495
Solomon, P. M., Downes, D., Radford, S. J. E., & Barrett, J. W. 1997, ApJ, 478, 144
Steidel, C. C., Shapley, A. E., Pettini, M., et al. 2004, ApJ, 604, 534
Swinbank, A. M., Smail, I., Chapman, S. C., et al. 2004, ApJ, 617, 64
Webb, T. M. A., Brodwin, M., Eales, S., & Lilly, S. J. 2004, ApJ, 605, 645